Innovative Infrastructure Solutions (2023) 8:328
https://doi.org/10.1007/s41062-023-01298-0

TECHNICAL PAPER

Behavior of a high-volume fly ash fiber-reinforced cement composite toward magnesium sulfate: a long-term study

H. K. Sugandhini[1] · Gopinatha Nayak[1] · Kiran K. Shetty[1] · Laxman P. Kudva[1]

Received: 20 August 2023 / Accepted: 28 October 2023 / Published online: 16 November 2023

Abstract

Sulfate attack is one of the severe concerns for concrete's durability in sulfate-rich soil, groundwater, and the marine environment. The ingress of dissolved sodium and (or) magnesium sulfate in concrete leads to the formation of expansive products such as gypsum, ettringite, brucite, and magnesium-silicate-hydrate (M–S–H), causing extensive cracking and disintegration of concrete based on the severity of the attack. The consequence of ingress of magnesium sulfate is more severe than sodium sulfate. The present article aims to assess the long-term behavior of a novel cement composite incorporating 80% class-F fly ash (F-FA) and 20% ordinary Portland cement with varying volume fractions of polypropylene fibers exposed to 5% magnesium sulfate solution for up to two years. The compressive strength, weight, and volume changes of the specimens measure these effects. The mixes with higher volume fractions of PP fibers undergo a 40% reduction in compressive strength, 6.7% weight gain, and 3.5% volume change at two years. The morphological features revealed through SEM images and EDX analysis find the formation of M–S–H, brucite, gypsum, ettringite traces, and unreacted F-FA. The outcomes of this study encourage the utilization of F-FA to a much higher volume to help reduce the carbon footprint and promote sustainability.

Keywords External sulfate attack · Magnesium sulfate · Polypropylene fibers · Microstructure, Cement replacement

Introduction

The ingress of sulfate ions significantly affects concrete's durability [1]. The internal source of sulfate is the raw materials used to produce concrete, and the external source of sulfates is the ingress of sulfate into the concrete through sulfate-rich soils and groundwater [2]. Both sources lead to the formation of expansive ettringite and induce matrix cracking. However, the internal sulfate attack depends on the temperature and slows down with time. In contrast, the external sulfate attack leads to more significant matrix deterioration with time due to the ability of sulfates to ingress concrete through the cracks [1–3]. In an external sulfate attack, the transfer of ions into concrete occurs in two modes: (i) ingress of sulfate into the cement matrix and (ii) deposition of leached calcium ions on the surface [4]. A combination of internal–external sulfate environments to assess the behavior of cast in-situ concrete reveals that internal sulfate attack severely damages the concrete due to extensive cracking that further worsens the member's condition due to the ingress of external sulfate ions [3].

Concrete exposed to marine environments experiences distress due to freeze–thaw cycles in the tidal zone and sulfate attack in the submerged area. The type and concentration of the solution influence the behavior of concrete. 5% magnesium sulfate solution damages the concrete more severely than 5% sodium sulfate solution [5]. A 3:1 dry–wet cycle ratio of sulfate exposure severely damages the concrete due to fatigue, causing changes in the concrete matrix [6]. The degradation of concrete due to chemical sulfate attack and physical sulfate attack is due to the mesoscopic pores. At an early age, i.e., within three months of exposure to a chemical sulfate attack, expansive products fill most mesoscopic pores. However, in a physical sulfate attack, the

✉ Laxman P. Kudva
laxman.kudva@manipal.edu

H. K. Sugandhini
sugandhini.hk@manipal.edu

Gopinatha Nayak
nayak.gopinatha@manipal.edu

Kiran K. Shetty
kiran.shetty@manipal.edu

[1] Department of Civil Engineering, Manipal Institute of Technology, Manipal Academy of Higher Education, Manipal, Karnataka 576104, India

expansive products occupy larger pores [7]. Ettringite forms both in capillary and gel pores. Crystallization of ettringite followed by expansion is associated with pore invasion and deformation [8–10].

Influence of incorporating SCMs toward resistance to sulfate attack

Alkali-activated concretes incorporating ground granulated blast furnace slag (GGBFS) and F-FA subjected to different forms of external sulfate of varying concentration solutions reveal that concretes combining GGBFS and F-FA offer better resistance to mass loss and length change [11]. F-FA's type, chemical composition, and fineness impact the desired characteristics of concrete at early and later ages [12–16]. Adding calcium hydroxide as an additive enhances the pozzolanic reaction of F-FA in concrete. The behavior of high-volume F-FA concrete depends on its fineness and the dosage of additives such as metakaolin and silica fume. Using ultra-fine F-FA improves the reactivity and properties of such concretes [17]. Combined freeze–thaw cycles and sulfate attack on concrete show that adding about 10% F-FA reduces the proportion of micro and capillary pores. However, excessive concentration of sodium sulfate coupled with high-frequency freeze–thaw cycles lead to the formation of more macro pores [18].

Using F-FA and nano-silica reduces pore size and enhances the microstructure and mechanical properties of the concrete [19]. However, the concretes incorporating nano-silica and silica fume blends exhibit brittle behavior [20]. Adding low volume F-FA, about 30%, reduces the pore diameter and aids in the densification of the matrix [21]. A blend of F-FA, silica fume, and nano-silica with OPC promises improved characteristics of concrete due to enhanced microstructure and reduced initial width of the micro-crack [22]. Adding 30%, F-FA reduces compressive strength and decreases water absorption [23].

An engineered cement composite containing varying ratios of F-FA to cement and a low volume of bentonite tested for resistance to wet/dry and sulfate solution reveals that an increase in F-FA to cement ratio reduces the resistance of the composite to sulfate solution. The addition of bentonite contributes to enhanced microstructure [24, 25]. Nano-engineered cement composite incorporating F-FA (30–50%) and 6% silica fume, tested under 5% magnesium sulfate solution, shows that adding 3% silica nanoparticles improves the mechanical and durability performance [26]. Adopting wet grinding of F-FA enhances the resistance to sulfate when the levels of F-FA are 50% of cement in heat-cured concretes [27]. The recent trends reveal the utilization of alternative coarse and fine aggregates such as Ferro Nickel Slag (FNS), Recycled Coarse aggregate (RCA), and Coal Bottom Ash (CBA) to produce sustainable concretes to conserve natural resources [28, 29].

Influence of F-FA and fibers in cement mortar, cement concrete, and cement composite toward sulfate attack

The issue of decalcification of C–S–H with the sulfate ions from external sources led to the utilization of supplementary cementitious materials (SCMs) such as class F-FA and GGBFS [8, 11, 17, 30]. The impact of incorporating 10% F-FA, basalt, and PP fibers in concrete offers better resistance to sulfate attack due to pore refinement measured using fractal dimension [31]. A high-volume F-FA of about 70% in self-compacting concrete helps improve the resistance toward sulfate attack. The SEM observation of samples of concrete containing 0–40% F-FA reveals the formation of fibrous C–S–H, crystals of calcium hydroxide, and needle-like ettringite. The concrete with 60% F-FA does not show the presence of ettringite [32]. Cement composite using ternary blends as a binder and hybrid fibers in the form of carbon nanotube, polyvinyl, and PP fibers show that using metakaolin reduces the permeability of the cement composite significantly. However, using PP fibers increases porosity and carbon nanotubes improve the behavior of cement composite toward magnesium sulfate solution [33].

Binary blends of F-FA and nano-silica with polyvinyl alcohol fibers in 1% by volume improve the mechanical properties and resistance to sodium sulfate solution [34]. Using wheat husk ash, rice husk ash, and glass powder in an F-FA-based cement composite with fibrillated PP fibers shows that a composite containing rice husk ash exhibits lesser mass loss than other mixes [35]. The influence of air entrainment on concrete mixes using 20% high calcium fly ash offers better resistance when subjected to a 5% sodium sulfate solution [36]. Incorporating 0.25% PP fibers by weight of the binder, air-cooled slag aggregate at 50% replacement to fine aggregate, and 45% F-FA as a substitute to cement in concrete offers better resistance to sulfate attack [37]. Microfibers of different lengths with lower volumes of F-FA show that 12 mm length and 20% combination impart better durability to concrete [38].

Incorporating F-FA and steel fibers in self-consolidating concrete exposed to dry–wet sulfate attack reveals that 50% F-FA is optimum for a dense microstructure [39]. The hybrid steel, glass, and PP fibers improves the resistance toward 5% sodium sulfate solution [40]. Utilizing PP fibers in concretes prone to freeze–thaw cycles and sulfate erosion shows that PP fibers in higher volume fractions

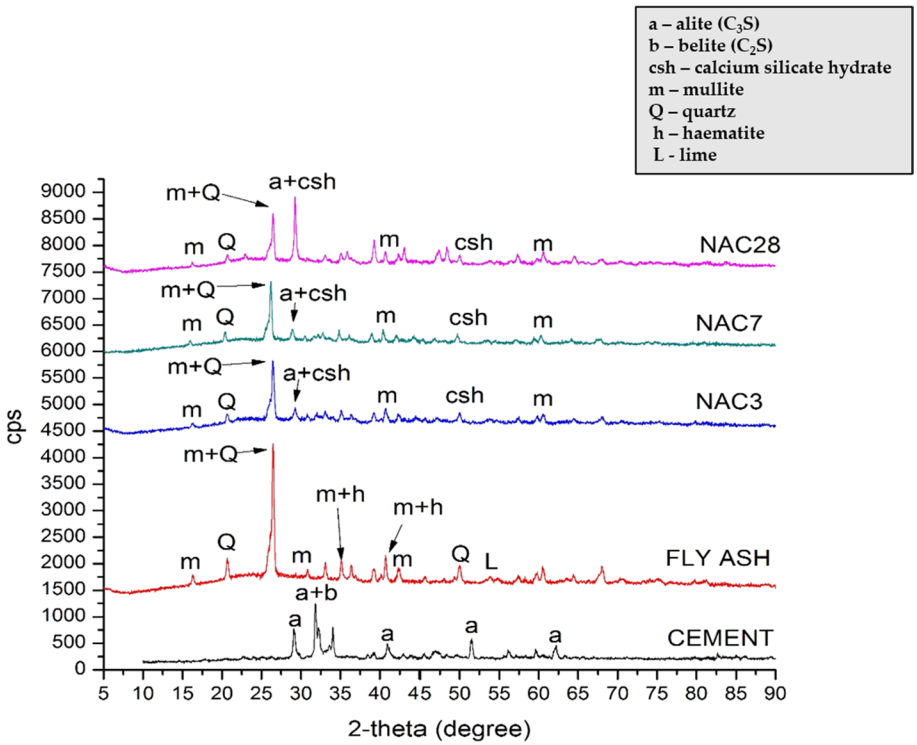

Fig. 1 XRD results of cement, F-FA, and NAC cured for 3, 7, and 28 days [48]

Table 1 Mix proportion of NAC with and without fibers in kg/m^3 [48]

Mix. no	Name	Cement	Fly ash	Water	Admixture	Fibers
M1	NAC	325	1300	243.75	6.5	0
M2	NAC PP 0.6	325	1300	243.75	6.5	5.52
M3	NAC PP 0.8	325	1300	243.75	6.5	7.36
M4	NAC PP 1.0	325	1300	243.75	6.5	9.2

improve the concrete's capacity to resist expansion due to the formation of gypsum and ettringite [41]. Adding nano-silica and PP fiber in alkali-activated concrete offers poor resistance to magnesium sulfate solution by severely affecting the flexural and compressive strength [42]. Concrete incorporating F-FA, bentonite, and polyvinyl fibers exhibits superior resistance to wet/dry cycles coupled with sulfate exposure due to the ability of F-FA to reduce the proportion of micropores [43].

Using recycled aggregates, F-FA, and PP fibers in concrete subjected to magnesium sulfate solution reveals that concretes with 0% recycled aggregates, 6% PP fibers, and 25% F-FA offer the best resistance [44]. Adding nano silica, nano titanium oxide, and PP fibers to concrete helps to improve the resistance to freeze–thaw cycles and sulfate attacks due to the bridging effect of PP fibers, thereby improving durability by 67% [45]. Using cellulose fibers in concrete with varying F-FA(0–30%) to assess the performance under dry–wet sulfate attack reveals that incorporating 30% F-FA reduces the resistance to sulfate solution [46]. Literature on incorporating fibers and SCMs to produce fiber-reinforced cement composite is widely available. However, there is a lack of studies to understand the behavior of fiber, matrix, and the long-term influence of fiber–matrix interface toward resistance to magnesium sulfate environment [47].

Summary of literature

Extensive studies on concrete, cement composite, and mortars incorporating various SCMs and fibers subjected to sodium and magnesium sulfate solutions of concentration varying between 5 and 10% for about 180 days are available with emphasis on the behavior under coupled attack (freeze–thaw and sulfate). However, the research on high-volume fly ash-based composites and high-volume fractions of PP fibers is limited. Most articles supplement the behavior under aggressive environments by conducting microstructure studies. The parameters considered to assess the behavior of samples subjected to sulfate exposure are compressive,

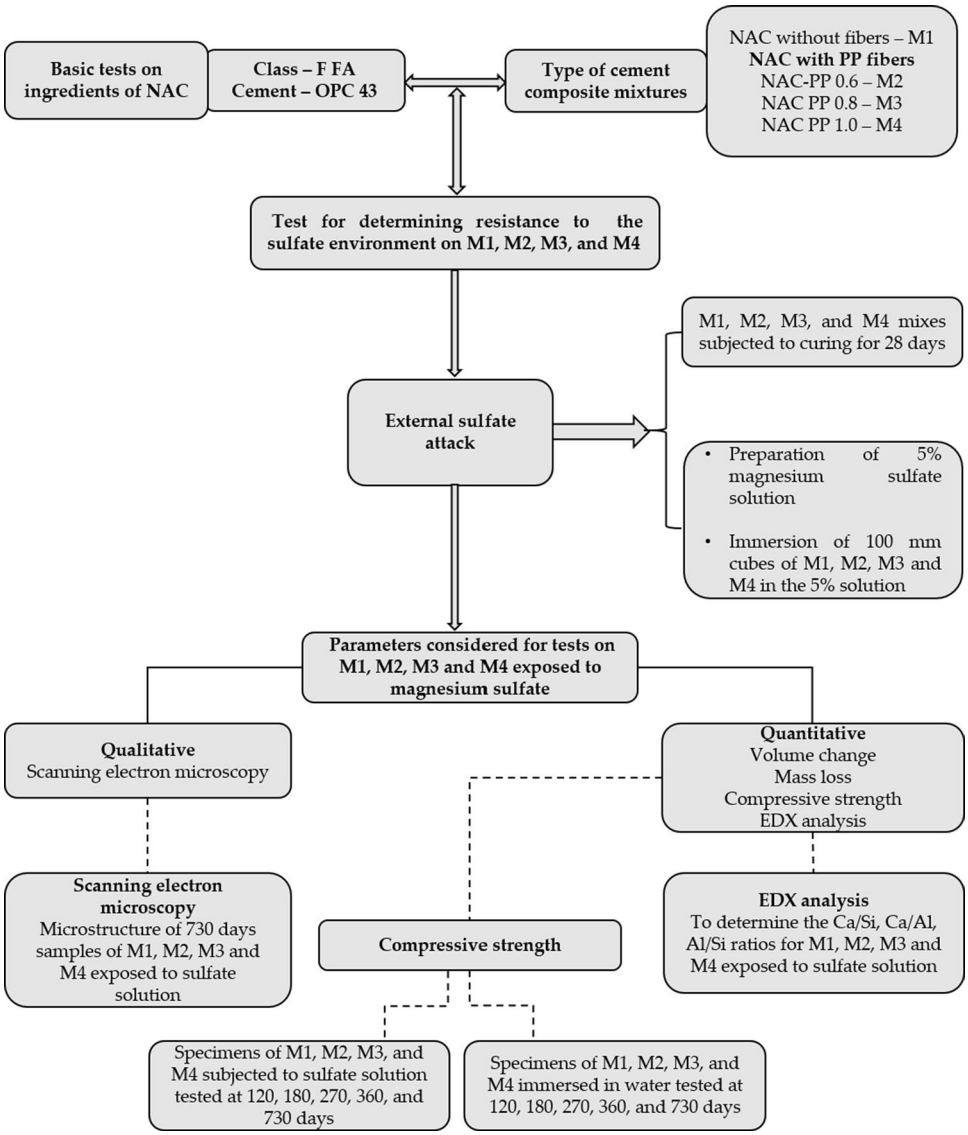

Fig. 2 Research Methodology

flexure, and splitting tensile strengths, mass loss, and microstructure analysis.

Scope of the present study

The article aims to assess the durability of a novel high-volume fly ash cement composite, the no-aggregate concrete (NAC), incorporating about 80% F-FA and 20% OPC with synthetic fibers in three different proportions from 0.6 to 1.0% toward external sulfate attack. Compressive strength, weight, and volume changes of 100 mm cubes immersed in the aggressive sulfate environment by preparing a 5% magnesium sulfate solution for up to two years are measured. The SEM images and EDX analysis correlate the morphological findings with the experimental results that show the exceptional potential of NAC with fibers toward magnesium sulfate attack in the long term.

Materials and methods

The present work uses OPC 43 grade cement, a high volume of F-FA of about 80%, potable water, PP fibers in three volume fractions, and a polycarboxylic ether (PCE) based plasticizer to achieve a low water–binder ratio. Figure 1 presents the mineralogical characterization using X-ray diffraction. PP fibers of length 12 mm, diameter 40 µm, relative density of 0.92, and tensile strength of 800 MPa are used for producing mixes M2, M3, and M4. Table 1 presents the mix proportions of NAC with 0, 0.6, 0.8, and 1.0% volume fractions of PP fibers.

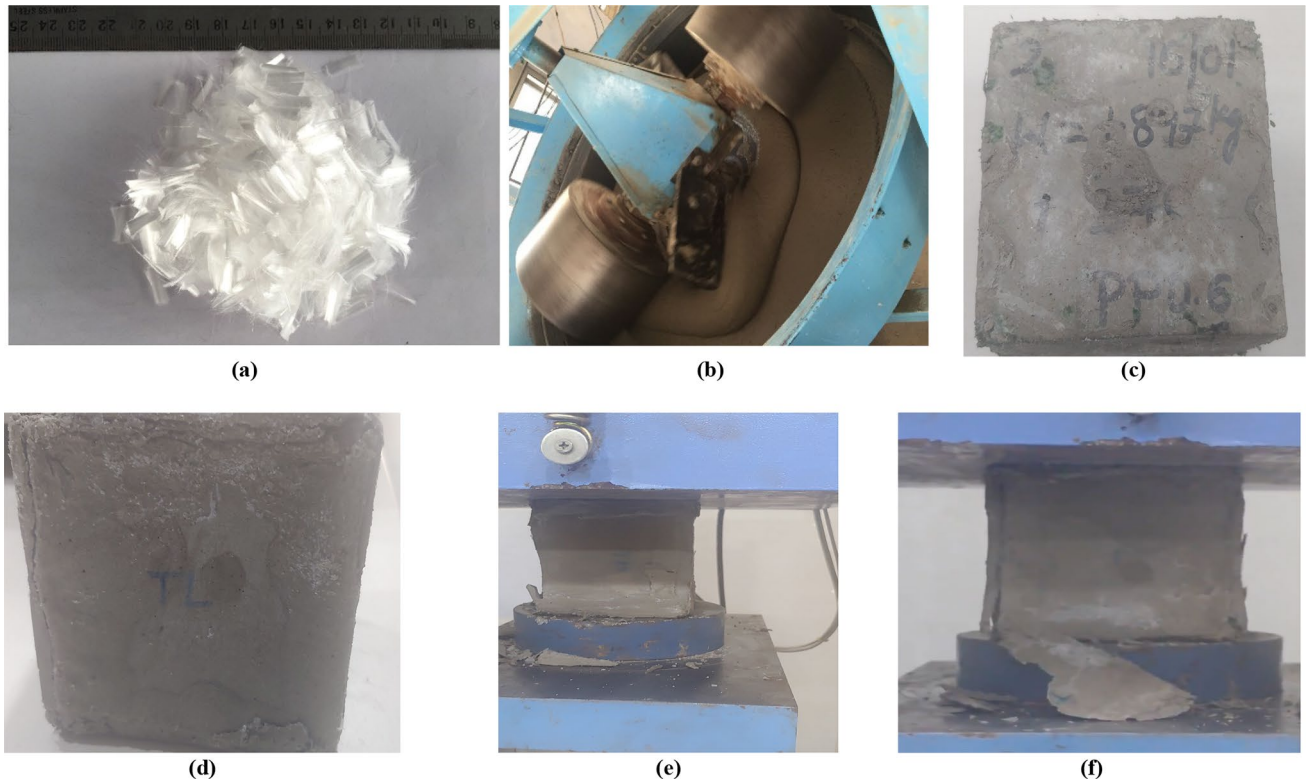

Fig. 3 **a** Polypropylene fibers used for preparing mixes M2, M3, and M4 **b** mixing process and the type of mixer for preparing the mixes, **c** sample specimen of M2 after 730 days exposure to sulfate, **d** expansion of sample M1 subjected to sulfate solution for 730 days **e** sample specimen under compression **f** spalling of a layer of M1 under compression after exposure to 730 days

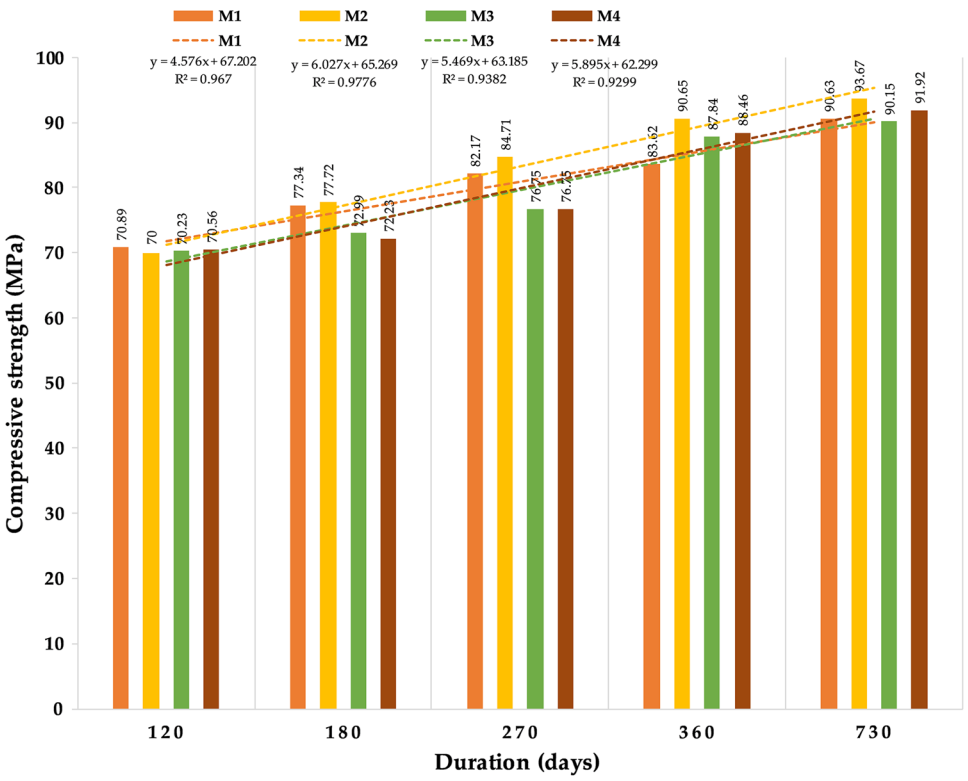

Fig. 4 Compression test results of NAC mixes with and without PP fibers immersed in water

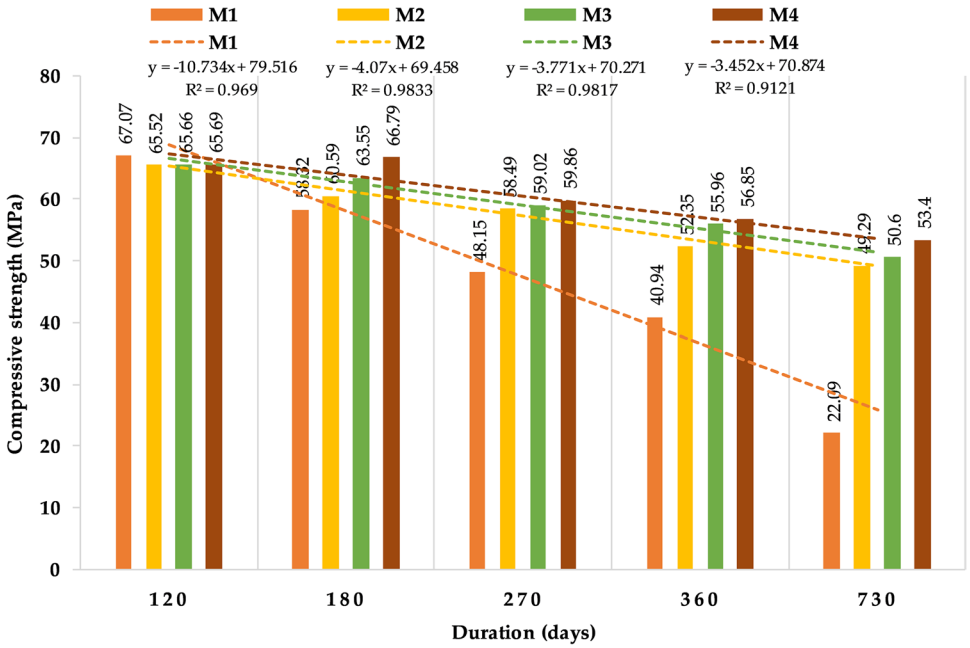

Fig. 5 Compression test results of NAC mixes with and without PP fibers exposed to sulfate solution

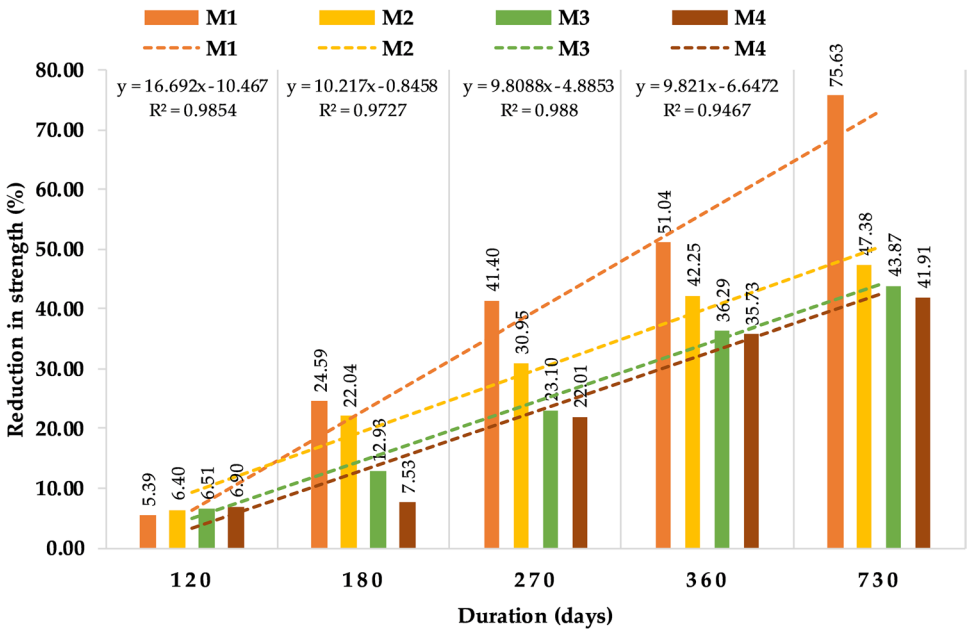

Fig. 6 Reduction in compressive strength of mixes M1, M2, M3 and M4

Methods

Figure 2 presents the research methodology designed to conduct the experimental investigation.

100 mm cubes of NAC with 0, 0.6, 0.8, and 1.0% PP fibers are cured under immersion for 28 days. These specimens are then exposed to the aggressive environment as a 5% magnesium sulfate solution for 120, 180, 270, 360, and 730 days. The weight, volume, and compressive strength changes are recorded for all specimens of each mix after each exposure duration. Microstructural studies such as SEM images and EDX analysis of samples exposed to sulfate solution for 730 days are conducted to observe the morphological changes and the presence of expansive products in the matrix. Figure 3 presents the preparation of the specimens. The compressive strength of the specimens immersed in (i) water and (ii) 5% magnesium sulfate solution for 120, 180, 270, 360, and 730 days is determined by loading the specimens under a compression testing machine of capacity 3000 kN at a

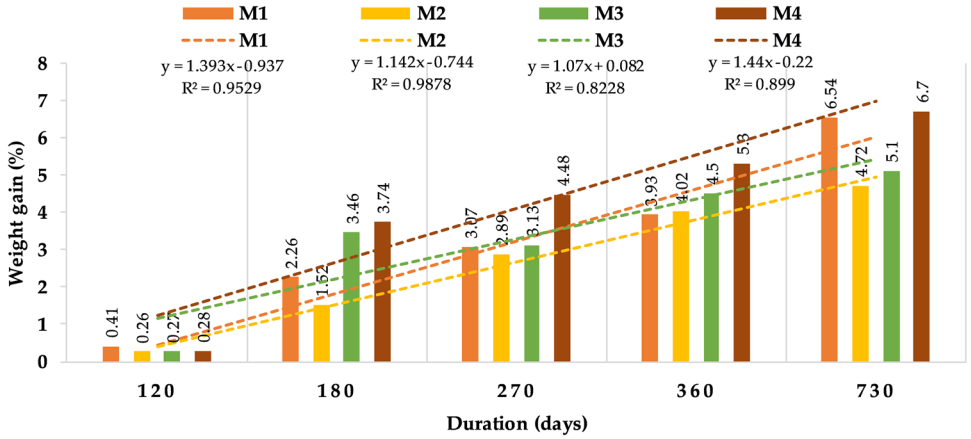

Fig. 7 Weight gain of mixes M1, M2, M3, and M4 exposed to sulfate environment

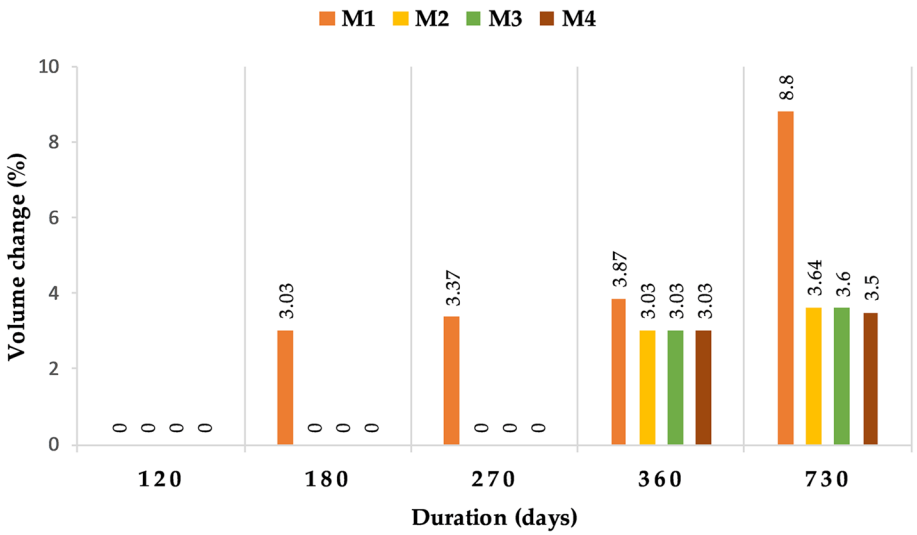

Fig. 8 Volume change of mixes M1, M2, M3, and M4 exposed to sulfate environment

rate as specified in IS 516:1959 [49]. The microstructure of samples exposed for 730 days to magnesium sulfate solution is studied.

Results and discussion

Compressive strength

Figures4 and 5 present the behavior of 100 mm cubes of NAC mixes M1, M2, M3, and M4 immersed in water and 5% magnesium sulfate solution for 120, 180, 270, 360, and 730 days under compression. The compression test results of specimens immersed in water show continuous gain in strength with time. Mix M1 attains an average compressive strength of 70.89 MPa at 120 days and 90.63 MPa at 730 days. M2's strength is 70 MPa at 120 days and 93.67 MPa at 730 days. The strength gain reduces with age, and there is less variation in compressive strength for mixes with fibers. M2 achieves the highest strength at all durations compared to all mixes. The strength gain follows a linear trend in all mixes with a high correlation value for R^2 above 0.9. The decrease in the rate of strength gain is due to the crystallization of hydration products that block water availability for further hydration. The availability of F-FA as a micro filler and dispersion of fibers reduces the possibility of water availability for the cement grains for hydration.

The mixes subjected to sulfate Attack by immersion in 5% magnesium sulfate solution show a reduction in strength with exposure. M1 experiences the highest loss in strength. Figure 5 shows the negative trend in strength gain with time.

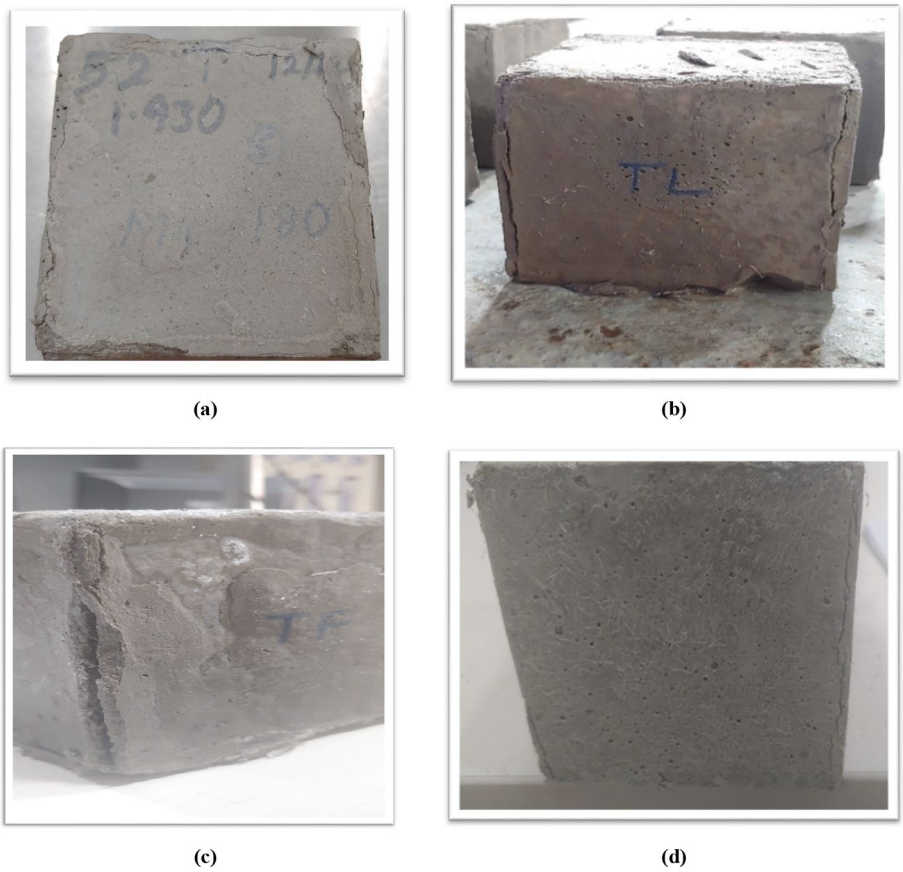

Fig. 9 Deformation of specimen at various duration **a** deformation of sample M1 at 180 days **b** deformation of sample M1 at 360 days **c** deformation of sample M1 at 730 days **d** deformation of sample M4 at 730 days

The mixes with fibers show lesser deterioration under sulfate attack as there is much less reduction in the compressive strength. The behavior of all mixes exposed to a sulfate environment follows a linear trend with a high correlation value of R^2 above 0.9. Utilization of PP fibers in higher volumes, i.e., 0.8 and 1.0% volume fraction, helps to hold the matrix intact and offers good resistance in long-term exposure to an aggressive sulfate environment.

Figure 6 presents the rate of reduction in compressive strength for the mixes exposed to sulfate solution in percentage. The decline in strength recorded for the mixes M1, M2, M3, and M4 at 120 days is 5.39%, 6.40%, 6.51%, and 6.90% respectively. Due to the weak fiber-matrix interface, the mixes with fibers experience a higher loss of strength at 120 days. With prolonged exposure to the sulfate environment, this trend reverses. While the mixes M2 and M1 show about 47% and 75% reduction, the M3 and M4 mixes exhibit about 40% strength reduction, showing the ability of fibers to hold the matrix intact despite the formation of expansive products. The addition of fibers also offers better resistance to crack propagation and the ability to resist the load under compression due to improvement in the fiber-matrix interface with time. Generally, the reduction rate sharply increases with time for all mixes and follows a linear trend with a high correlation value of R^2 above 0.9.

Weight gain and volume change

When subjected to a sulfate environment, the mixes with PP fibers show weight gain with time. Figure 7 presents the data for weight change observed in specimens for various exposure durations to magnesium sulfate solution. Mix M1 shows 0.41% weight gain at 120 days and 6.54% at 730 days. The values recorded for mixes M2, M3, and M4 are 0.26, 0.27, and 0.28%, respectively, indicating less variation at 120 days. With prolonged exposure to the sulfate environment, the mixes with fibers show higher weight gain. M4 gains the highest weight of 6.7% among all mixes at 730 days. All mixes follow a linear pattern, with an R^2 value above 0.8. Mix M2 has the best correlation with an R^2 value close to 1, followed by mix M1.

Figure 8 presents the volume change exhibited by the mixes exposed to sulfate solution for various durations. The specimens show no expansion or cracks at 120 days. M1 indicates a steady rise in volume change with 3.03%, 3.37%,

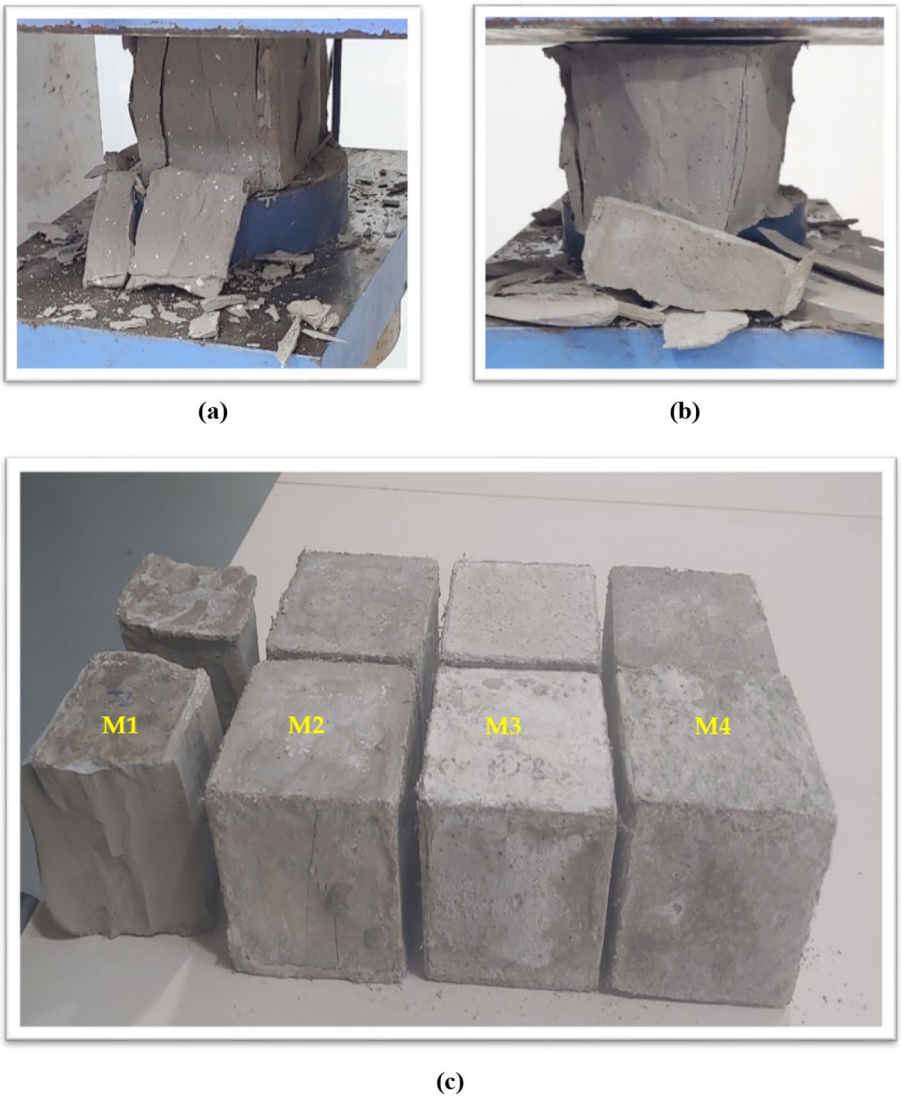

Fig. 10 Failure pattern of specimens at various duration **a** failure of sample M1 at 180 days **b** Failure of sample M1 at 360 days **c** Failure of samples M1, M2, M3, and M4 at 730 days

and 3.87% at 180, 270, and 360 days under sulfate exposure. In contrast, the mixes M2, M3, and M4 do not experience volume change till 270 days of exposure. However, at 360 and 730 days of exposure, M2, M3, and M4 experience a volume change of about 3.03–3.65%. About 8.8% volume change is observed at 730 days for mix M1 and is the highest among the mixes at 730 days.

Figures 9a, b, and c depict the physical deterioration of mix M1 at 180, 360, and 730 days respectively. M1 exposed to sulfate solution for 180 days exhibits chipped corners and slight cracks at the edges. The mixes with fibers do not show such disintegration. At 360 days, the deterioration of mix M1 due to the formation of expansive products is prominent in the form of wide cracks propagating throughout the specimen and affecting the composition of the matrix of M1, as shown in Fig. 9b. At 730 days, the sample shows extreme distress due to the corrosive products such as M–S–H and brucite, leading to the formation of large cracks, chipping of sides, losing homogeneity in appearance and cohesivity of the matrix, in turn contributing to spalling of the face of the specimen as shown in Fig. 9c. Contrary to mix M1, at 730 days, mix M4 shows slight cracks continuing from bottom to top along the sides with slight chipping at the edges, as presented in Fig. 9d.

Figures 10a and b present the failure pattern of M1 at 180 and 360 days under compression. The core of the specimen is intact, and the failure happens due to the spalling of the surface layers of the sample, denoting the inability of the sulfate ions to ingress into the core of the test specimen due to homogeneous and cohesive matrix and the ability of high-volume F-FA to reduce the pore size. The spalling is higher for M1 exposed to sulfate

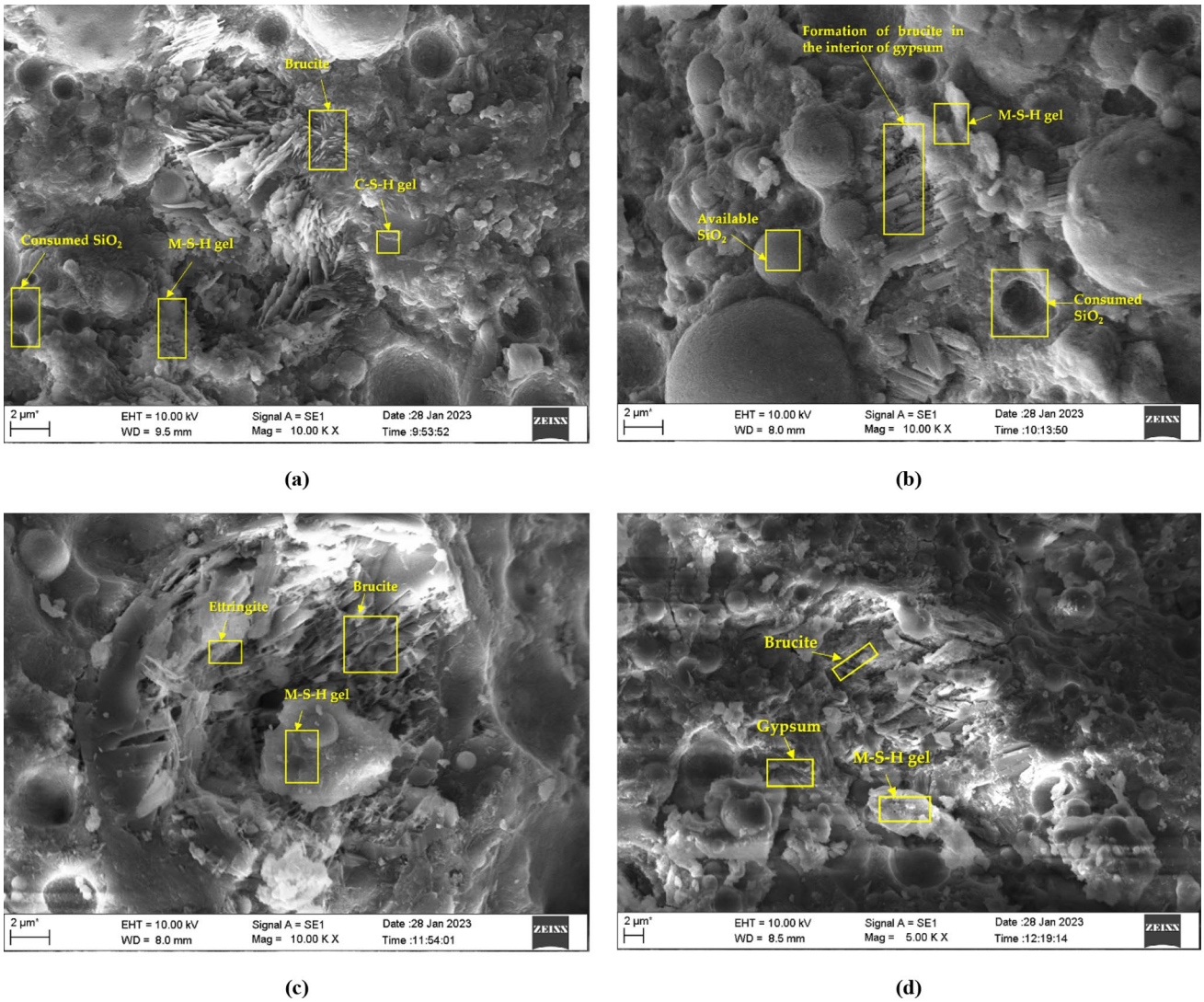

Fig. 11 Morphology of mix **a** M1 **b** M2 **c** M3 and **d** M4 after 730 days exposure to magnesium sulfate solution

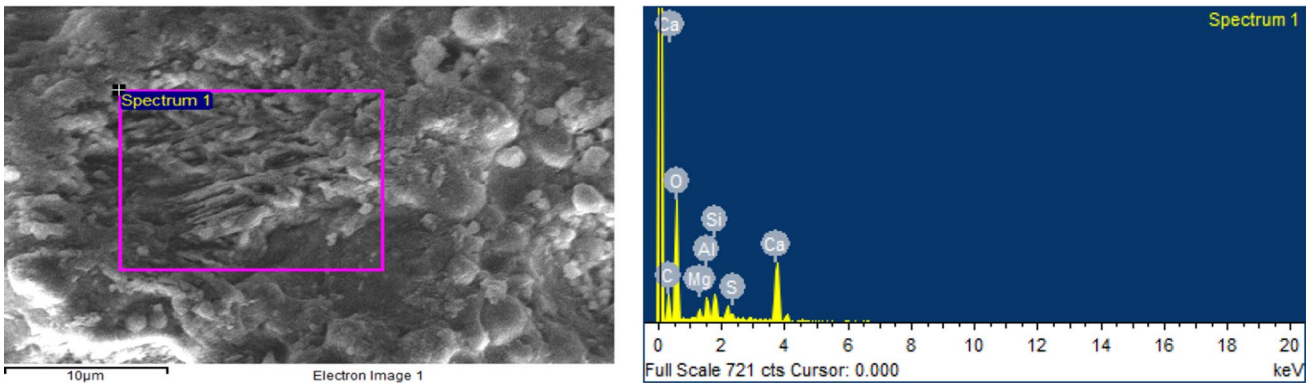

Fig. 12 EDX spectrum of mix M1 after 730 days exposure to sulfate environment

Table 2 Ratios of chief oxides in the mixes after exposure to the sulfate environment for 730 days

Mix type	CaO	SiO_2	Al_2O_3	Ca/Si	Ca/Al	Al/Si
M1	9.57	7.58	3.86	1.26	2.48	0.51
M2	6.84	5.69	3.4	1.20	2.01	0.60
M3	6.87	12.09	5.89	0.57	1.17	0.49
M4	8.81	12.07	7.06	0.73	1.25	0.58

solution for 360 days, indicating the higher deteriorating effect of magnesium sulfate on the composition of the matrix without fibers, as shown in Fig. 10b. Figure 10c shows the failure pattern of M1, M2, M3, and M4 under compression after 730 days of exposure to magnesium sulfate solution. The mixes with fibers do not display the signs of spalling despite cracks at the surface before testing and hence have a better ability to resist compression. The presence of fibers and their distribution help to hold the matrix intact by arresting the crack propagation and, in turn, reduces the width of the cracks in the mixes with fibers, i.e., M2, M3, and M4. The specimens with fibers do not lose cohesiveness despite prolonged exposure to the aggressive sulfate environment.

These observations indicate that mix M1 is highly susceptible to sulfate attack as the ability to hold the matrix intact is severely affected at 730 days despite using high-volume F-FA. The addition of PP fibers helps achieve discontinuity of capillary pores by acting as a barrier due to the distribution in the matrix. When used in higher volume fractions of about 0.8 and 1.0%, it prevents the disintegration of the matrix despite the formation of expansive products.

Morphological investigation

The subsequent section presents the microstructural studies in the form of SEM images and EDX analysis of mixes M1, M2, M3, and M4 subjected to sulfate attack for up to 730 days. Figure 11a displays the formation of brucite, magnesium silicate hydrate (M–S–H), calcium silicate hydrate (C–S–H), and many empty spherical pockets due to the consumption of SiO_2 to form M–S–H. The decalcification of C–S–H and the exchange reaction to replace calcium ions with magnesium leads to the loss of cohesivity of the matrix [11, 30, 50]. The absence of unreacted F-FA in the matrix also complements the formation of calcium sulfoaluminates.

The SEM observations for mixes with fibers show the presence of gypsum, ettringite, brucite, M–S–H, and C–S–H, as depicted in Figs. 11b, c, and d, respectively. The prominent observation in the mixes with fibers is the presence of unreacted F-FA particles, i.e., SiO_2, unlike M1. The matrix is cohesive in the mixes containing fibers, and the ability of unreacted F-FA particles to act as micro filler is validated. The dispersion of PP fibers and the availability of F-FA also act as a barrier to the ingress of the sulfate solution, enhancing the microstructure of the mixes M2, M3, and M4 [6, 41, 46, 51]. The presence of cracks is noticed in all the mixes irrespective of the addition of the fibers due to M–S–H and brucite causing the disintegration of the binder matrix. The formation of gypsum and ettringite aggravates the deterioration process due to the larger volume of these products, causing stress leading to expansion, cracking, and loss of strength.

Figure 12 presents the EDX spectrum of M1. It shows calcium, magnesium, aluminate, sulfate, and silicate as the chief elemental composition. Table 2 presents the ratios of chief oxides based on the atomic weight % obtained from the EDX. The ratio of Ca/Si is 1.26 and 1.20 for mix M1 and M2, respectively. The ratio reduces to 0.57 and 0.73 for mixes M3 and M4. For the Ca/Al ratio, a similar trend follows. The higher Ca/Si ratio indicates a reduction in the strength for M1 and M2, and a lower Ca/Si ratio indicates higher compressive strength for mixes M3 and M4. The Al/Si ratio for mixes ranges from 0.49 to 0.60, which supplements the reason for reduced strength with prolonged exposure to the sulfate environment.

Conclusions

This article presents the long-term durability of a novel cementitious composite with a high-volume fraction of PP fibers and F-FA under an aggressive sulfate environment. The key indicators used to evaluate the performance of mixes are changes in compressive strength, weight and volume, and microstructure characteristics. The important findings from this study are:

- The mix M1, after prolonged exposure to magnesium sulfate, performs poorly under compressive loads due to the spalling of the outer layers of the sample. However, the mixes with fibers show better results under compression due to the ability of fibers to disperse in the matrix and hold the matrix intact despite the formation of expansive products.
- NAC without fibers is highly susceptible to deterioration under sulfate exposure. A higher volume fraction of PP fibers, i.e., 0.8 and 1.0%, significantly improves

the resistance to sulfate attack due to higher residual strength.

- The fiber-matrix interface improves with time, leading to weight gain in mixes with 0.8 and 1.0% volume fraction PP fibers. The volume change is insignificant in these mixes despite prolonged exposure to the sulfate environment.
- The microstructure of mixes with fibers is generally cohesive, with unreacted F-FA acting as a micro filler.

These observations show that NAC with a higher volume fraction of PP fibers has immense potential to resist external sulfate attack and can be a choice for applications in environments with excess sulfate content.

Acknowledgements The authors credit the inventors, Dr. Bhanumathidas and N. Kalidas, Directors, INSWAREB, Vishakhapatnam, Andhra Pradesh, India, for allowing the authors to work on no-aggregate concrete and offering technical and technological support at various stages of the study. They hold the IP rights of no-aggregate concrete.

Author contributions SHK and GN contributed to Conceptualization; SHK contributed to methodology, investigation resources, writing—original draft preparation, writing—review and editing and supervision; SHK, KKS, and LKP contributed to data curation; GN contributed to visualization; GN and KKS contributed to project administration; All authors have read and agreed to the published version of the manuscript.

Funding This research received no external funding and The APC was funded by Manipal Academy of Higher Education, Manipal 576104, Karnataka, India.

Declarations

Conflict of interest The authors declare no conflict of interest.

Ethical approval This paper neither was published nor is under review elsewhere.

Informed consent All the authors are aware of this paper.

References

1. Tahwia AM, Fouda RM, AbdElrahman M, Youssf O (2022) Long-term performance of concrete made with different types of cement under severe sulfate exposure. Materials 16:240. https://doi.org/10.3390/ma16010240
2. Ouyang C, Nanni A, Chang WF (1988) Internal and external sources of sulfate ions in portland cement mortar: two types of chemical attack. Cem Concr Res 18:699–709. https://doi.org/10.1016/0008-8846(88)90092-0
3. Zhao G, Li J, Shi M, Fan H, Cui J, Xie F (2020) Degradation mechanisms of cast-in-situ concrete subjected to internal-external combined sulfate attack. Constr Build Mater 248:118683. https://doi.org/10.1016/j.conbuildmat.2020.118683
4. Ragoug R, Metalssi OO, Barberon F, Torrenti J-M, Roussel N, Divet L, d'Espinose De Lacaillerie J-B (2019) Durability of cement pastes exposed to external sulfate attack and leaching: physical and chemical aspects. Cem. Concr. Res. 116:134–145. https://doi.org/10.1016/j.cemconres.2018.11.006
5. Wang R, Zhang Q, Li Y (2022) Deterioration of concrete under the coupling effects of freeze-thaw cycles and other actions: a review. Constr Build Mater 319:126045. https://doi.org/10.1016/j.conbuildmat.2021.126045
6. Wang K, Guo J, Wu H, Yang L (2020) Influence of dry-wet ratio on properties and microstructure of concrete under sulfate attack. Constr Build Mater 263:120635. https://doi.org/10.1016/j.conbuildmat.2020.120635
7. Zhang Z, Zhou J, Yang J, Zou Y, Wang Z (2020) Understanding of the deterioration characteristic of concrete exposed to external sulfate attack: insight into mesoscopic pore structures. Constr Build Mater 260:119932. https://doi.org/10.1016/j.conbuildmat.2020.119932
8. Gu Y, Dangla P, Martin R-P, OmikrineMetalssi O, Fen-Chong T (2022) Modeling the sulfate attack induced expansion of cementitious materials based on interface-controlled crystal growth mechanisms. Cem Concr Res 152:106676. https://doi.org/10.1016/j.cemconres.2021.106676
9. Gu Y, Martin R-P, OmikrineMetalssi O, Fen-Chong T, Dangla P (2019) Pore size analyzes of cement paste exposed to external sulfate attack and delayed ettringite formation. Cem Concr Res 123:105766. https://doi.org/10.1016/j.cemconres.2019.05.011
10. Liu P, Chen Y, Wang W, Yu Z (2020) Effect of physical and chemical sulfate attack on performance degradation of concrete under different conditions. Chem Phys Lett 745:137254. https://doi.org/10.1016/j.cplett.2020.137254
11. Bondar D, Nanukuttan S (2022) External sulfate attack on alkali-activated slag and slag/fly ash concrete. Buildings 12:94. https://doi.org/10.3390/buildings12020094
12. Nayak DK, Abhilash PP, Singh R, Kumar R, Kumar V (2022) Fly ash for sustainable construction: a review of fly ash concrete and its beneficial use case studies. Clean Mater 6:100143. https://doi.org/10.1016/j.clema.2022.100143
13. Rida L, Alaoui AH (2022) Effect of high volume fly ash and curing temperature on delayed ettringite formation. Mater Today Proc 58:1285–1293. https://doi.org/10.1016/j.matpr.2022.02.110
14. Juenger MC, Siddique R (2015) Recent advances in understanding the role of supplementary cementitious materials in concrete. Cem Concr Res 78:71–80
15. Tang SW, Yao Y, Andrade C, Li ZJ (2015) Recent durability studies on concrete structure. Cem Concr Res 78:143–154
16. Lothenbach B, Scrivener K, Hooton RD (2011) Supplementary cementitious materials. Cem Concr Res 41:1244–1256. https://doi.org/10.1016/j.cemconres.2010.12.001
17. Herath C, Gunasekara C, Law DW, Setunge S (2020) Performance of high volume fly ash concrete incorporating additives: a systematic literature review. Constr Build Mater 258:120606. https://doi.org/10.1016/j.conbuildmat.2020.120606
18. Tian W, Gao F (2020) Damage and degradation of concrete under coupling action of freeze-thaw cycle and sulfate attack. Adv Mater Sci Eng 2020:1–17. https://doi.org/10.1155/2020/8032849
19. Golewski GL (2022) Combined effect of coal fly ash (CFA) and nanosilica (NS) on the strength parameters and microstructural properties of eco-friendly concrete. Energies 16:452. https://doi.org/10.3390/en16010452
20. Golewski GL (2023) Concrete composites based on quaternary blended cements with a reduced width of initial microcracks. Appl Sci 13:7338. https://doi.org/10.3390/app13127338
21. Golewski GL (2023) Assessing of water absorption on concrete composites containing fly ash up to 30% in regards to structures completely immersed in water. Case Stud Constr Mater 19:e02337. https://doi.org/10.1016/j.cscm.2023.e02337

22. Golewski GL (2023) Mechanical properties and brittleness of concrete made by combined fly ash, silica fume and nanosilica with ordinary portland cement. AIMS Mater Sci 10:390–404. https://doi.org/10.3934/matersci.2023021
23. Golewski GL (2023) The effect of the addition of coal fly ash (CFA) on the control of water movement within the structure of the concrete. Materials 16:5218. https://doi.org/10.3390/ma16155218
24. Quan X, Wang S, Liu K, Zhao N, Xu J, Xu F, Zhou J (2021) The Corrosion resistance of engineered cementitious composite (ECC) containing high-volume fly ash and low-volume bentonite against the combined action of sulfate attack and dry-wet cycles. Constr Build Mater 303:124599. https://doi.org/10.1016/j.conbuildmat.2021.124599
25. Zhao N, Wang S, Wang C, Quan X, Yan Q, Li B (2020) Study on the durability of engineered cementitious composites (ECCs) containing high-volume fly ash and bentonite against the combined attack of sulfate and freezing–thawing (F–T). Constr Build Mater 233:117313. https://doi.org/10.1016/j.conbuildmat.2019.117313
26. Singh LP, Ali D, Tyagi I, Sharma U, Singh R, Hou P (2019) Durability studies of nano-engineered fly ash concrete. Constr Build Mater 194:205–215. https://doi.org/10.1016/j.conbuildmat.2018.11.022
27. Yang J, Zeng L, He X, Su Y, Li Y, Tan H, Jiang B, Zhu H, Oh S-K (2021) Improving durability of heat-cured high volume fly ash cement mortar by wet-grinding activation. Constr Build Mater 289:123157. https://doi.org/10.1016/j.conbuildmat.2021.123157
28. Saxena A, Sulaiman SS, Shariq M, Ansari MA (2023) Experimental and analytical investigation of concrete properties made with recycled coarse aggregate and bottom ash. Innov Infrastruct Solut 8:197. https://doi.org/10.1007/s41062-023-01165-y
29. Irmawaty R, Caronge MA, Tjaronge MW, Abdurrahman MA, Ahmad SB (2023) Compressive strength and corrosion behavior of steel bars embedded in concrete produced with ferronickel slag aggregate and fly ash: an experimental study. Innov Infrastruct Solut 8:200. https://doi.org/10.1007/s41062-023-01162-1
30. Elahi MMA, Shearer CR, Naser Rashid Reza A, Saha AK, Khan MNN, Hossain MM, Sarker PK (2021) Improving the sulfate attack resistance of concrete by using supplementary cementitious materials (SCMs): a review. Constr Build Mater 281:122628. https://doi.org/10.1016/j.conbuildmat.2021.122628
31. Zhang J, Zheng Q, Cheng M (2021) Study on mechanical properties and air-void structure characteristics of hybrid fiber fly ash concrete under sulfate attack. Mater Res Express 8:105504. https://doi.org/10.1088/2053-1591/ac2d6e
32. Liu J, Li A, Yang Y, Wang X, Yang F (2022) Dry–wet cyclic sulfate attack mechanism of high-volume fly ash self-compacting concrete. Sustainability 14:13052. https://doi.org/10.3390/su142013052
33. Mansoori A, Behfarnia K (2021) Evaluation of mechanical and durability properties of engineered cementitious composites exposed to sulfate attack and freeze-thaw cycle. Asian J Civ Eng 22:417–429. https://doi.org/10.1007/s42107-020-00322-3
34. Huang J, Wang Z, Li D, Li G (2022) Effect of nano-SiO2/PVA fiber on sulfate resistance of cement mortar containing high-volume fly ash. Nanomaterials 12:323. https://doi.org/10.3390/nano12030323
35. Hanif Khan M, Zhu H, Ali Sikandar M, Zamin B, Ahmad M, Sabri M (2022) Effects of various mineral admixtures and fibrillated polypropylene fibers on the properties of engineered cementitious composite (ECC) based mortars. Materials 15:2880. https://doi.org/10.3390/ma15082880
36. Jaworska-Wędzińska M, Jasińska I (2021) Durability of mortars with fly ash subject to freezing and thawing cycles and sulfate attack. Materials 15:220. https://doi.org/10.3390/ma15010220
37. Kim J, Qudoos A, Jakhrani S, Lee J, Kim S, Ryou J-S (2019) Mechanical properties and sulfate resistance of high volume fly ash cement mortars with air-cooled slag as fine aggregate and polypropylene fibers. Materials 12:469. https://doi.org/10.3390/ma12030469
38. Görhan G, Kavasoğlu E (2022) Effect of fly ash on mechanical and durability properties of mortar containing microfibers with different length. Eur J Environ Civ Eng 26:1283–1299. https://doi.org/10.1080/19648189.2019.1707713
39. Liu J, Zang S, Yang F, Zhang M, Li A (2022) Fracture mechanical properties of steel fiber reinforced self-compacting concrete under dry-wet cycle sulfate attack. Buildings 12:1623. https://doi.org/10.3390/buildings12101623
40. Bankir MB, KorkutSevim U (2020) Performance optimization of hybrid fiber concretes against acid and sulfate attack. J Build Eng 32:101443. https://doi.org/10.1016/j.jobe.2020.101443
41. Gong L, Yu X, Liang Y, Gong X, Du Q (2023) Multi-scale deterioration and microstructure of polypropylene fiber concrete by salt freezing. Case Stud Constr Mater 18:e01762. https://doi.org/10.1016/j.cscm.2022.e01762
42. Hussein TA, Dheyaaldin MH, Mosaberpanah MA, Ahmed YMS, Mohammed HA, Omer RR, Hamid SM, Alzeebaree R (2023) Chemical resistance of alkali-activated mortar with nano silica and polypropylene fiber. Constr Build Mater 363:129847. https://doi.org/10.1016/j.conbuildmat.2022.129847
43. Zhao N, Wang S, Quan X, Liu K, Xu J, Xu F (2022) Behavior of fiber reinforced cementitious composites under the coupled attack of sulfate and dry/wet in a tidal environment. Constr Build Mater 314:125673. https://doi.org/10.1016/j.conbuildmat.2021.125673
44. YavuzBayraktar O, Salem TaherEshtewı S, Benli A, Kaplan G, Toklu K, Gunek F (2021) The Impact of RCA and fly ash on the mechanical and durability properties of polypropylene fiber-reinforced concrete exposed to freeze-thaw cycles and MgSO4 with ANN modeling. Constr Build Mater 313:125508. https://doi.org/10.1016/j.conbuildmat.2021.125508
45. Ren J, Lai Y (2021) Study on the durability and failure mechanism of concrete modified with nanoparticles and polypropylene fiber under freeze-thaw cycles and sulfate attack. Cold Reg Sci Technol 188:103301. https://doi.org/10.1016/j.coldregions.2021.103301
46. Wei Y, Chai J, Qin Y, Li Y, Xu Z, Li Y, Ma Y (2021) Effect of fly ash on mechanical properties and microstructure of cellulose fiber-reinforced concrete under sulfate dry–wet cycle attack. Constr Build Mater 302:124207. https://doi.org/10.1016/j.conbuildmat.2021.124207
47. Ma H, Yi C, Wu C (2021) Review and outlook on durability of engineered cementitious composite (ECC). Constr Build Mater 287:122719. https://doi.org/10.1016/j.conbuildmat.2021.122719
48. Sugandhini HK, Nayak G, Shetty KK, Kudva LP (2023) the durability of high-volume fly ash-based cement composites with synthetic fibers in a corrosive environment: a long-term study. Sustainability 15:11481. https://doi.org/10.3390/su151511481
49. IS 516 (1959): Method of Tests for Strength of Concrete. Bureau of Indian Standards: Chandigarh, India
50. Aye T, Oguchi CT, Takaya Y (2010) Evaluation of sulfate resistance of portland and high alumina cement mortars using hardness test. Constr Build Mater 24:1020–1026. https://doi.org/10.1016/j.conbuildmat.2009.11.016
51. Shen Y, Li Q, Huang B, Liu X, Xu S (2022) Effects of PVA fibers on microstructures and hydration products of cementitious composites with and without fly ash. Constr Build Mater 360:129533. https://doi.org/10.1016/j.conbuildmat.2022.129533